THE JOURNAL OF BIOLOGICAL CHEMISTRY VOL. 290, NO. 13, pp. 8396–8408, March 27, 2015

Distinct Mechanisms of Recognizing Endosomal Sorting Complex Required for Transport III (ESCRT-III) Protein IST1 by Different Microtubule Interacting and Trafficking (MIT) Domains*

Received for publication, August 28, 2014, and in revised form, February 2, 2015 Published, JBC Papers in Press, February 5, 2015, DOI 10.1074/jbc.M114.607903

Emily Z. Guo[‡] **and Zhaohui Xu**[‡§1]

From the [‡]*Life Science Institute and* [§]*Department of Biological Chemistry, Medical School, University of Michigan, Ann Arbor, Michigan 48109*

Background: IST1 recruits MIT domain-containing proteins VPS4, LIP5, and Spartin to the mid-body during cytokinesis.
Results: Crystal structures of IST1 in complex with VPS4, LIP5, or Spartin were determined.
Conclusion: IST1 binds to structurally similar MIT domains using two distinct mechanisms.
Significance: This study elucidated for the first time the structural basis that determines the specificity in IST1-MIT domain interaction.

The endosomal sorting complex required for transport (ESCRT) machinery is responsible for membrane remodeling in a number of biological processes including multivesicular body biogenesis, cytokinesis, and enveloped virus budding. In mammalian cells, efficient abscission during cytokinesis requires proper function of the ESCRT-III protein IST1, which binds to the microtubule interacting and trafficking (MIT) domains of VPS4, LIP5, and Spartin via its C-terminal MIT-interacting motif (MIM). Here, we studied the molecular interactions between IST1 and the three MIT domain-containing proteins to understand the structural basis that governs pairwise MIT-MIM interaction. Crystal structures of the three molecular complexes revealed that IST1 binds to the MIT domains of VPS4, LIP5, and Spartin using two different mechanisms (MIM1 mode *versus* MIM3 mode). Structural comparison revealed that structural features in both MIT and MIM contribute to determine the specific binding mechanism. Within the IST1 MIM sequence, two phenylalanine residues were shown to be important in discriminating MIM1 *versus* MIM3 binding. These observations enabled us to deduce a preliminary binding code, which we applied to provide CHMP2A, a protein that normally only binds the MIT domain in the MIM1 mode, the additional ability to bind the MIT domain of Spartin in the MIM3 mode.

The endosomal sorting complex required for transport (ESCRT)[2] is an evolutionarily conserved molecular machine that functions to sculpt biological membranes to produce curvature away from the cytoplasm (1–4). It is required for a number of important biological processes, including intraluminal vesicle formation during multivesicular body biogenesis (5), budding of enveloped viruses (6), abscission during cytokinesis (7), and repair of small plasma membrane wounds (8). The ESCRT machinery consists of a series of protein complexes, including ESCRT-0, -I, -II, -III, and VPS4 complexes (9, 10). They are assembled, activated and eventually disassembled in an orderly and timely fashion during ESCRT activity. Specific protein-protein interactions involving modular protein binding domains play important roles in these processes. Some of these interactions are mediated by microtubule interacting and trafficking (MIT) domains (11). The MIT domain consists of a trihelical structural fold and binds short peptide sequences collectively known as the "MIT-interacting motifs" (MIMs).

In the ESCRT machinery, MIMs have been identified at the C-terminal ends of proteins that belong to the ESCRT-III complex (12, 13). There are four major ESCRT-III proteins: CHMP2 (yeast ortholog: Vps2), CHMP3 (Vps24), CHMP4 (Snf7), and CHMP6 (Vps20) (12). They share a common structural fold that includes an N-terminal core helical domain and a C-terminal region that includes the MIM sequence (14). In their inactive state, the ESCRT-III proteins are kept as monomeric, soluble proteins in the cytosol by engaging the C-terminal regions in intramolecular interactions with their N-terminal core domains (13, 15, 16). Upon activation, they oligomerize to form the ESCRT-III complex (17, 18), which is directly responsible for generating membrane curvature and likely catalyzing the vesicle scission reaction as well (19, 20). In addition to the four major ESCRT-III proteins, there are at least three ESCRT-III related proteins: CHMP1 (Did2), CHMP5 (Vps60), and IST1 (Ist1). Although their structures are similar to that of an ESCRT-III protein, they are generally not considered to be major structural components of the membrane-bound ESCRT-III complex but instead play important regulatory roles for the ESCRT machinery function (21–28).

Membrane-bound ESCRT-III proteins are removed and recycled into the cytosol at the end of the vesicle budding reaction cycle, a process catalyzed by the AAA-ATPase VPS4

* This work was supported, in whole or in part, by National Institutes of Health Grant GM095769 (to Z. X.).
The atomic coordinates and structure factors (codes 4U7I, 4U7Y, and 4U7E) have been deposited in the Protein Data Bank (http://wwpdb.org/).
[1] To whom correspondence should be addressed: 210 Washtenaw Ave., Life Sciences Institute, University of Michigan, Ann Arbor, MI 48109. Tel.: 734-615-2077; Fax: 734-763-6492; E-mail: zhaohui@umich.edu.
[2] The abbreviations used are: ESCRT, endosomal sorting complex required for transport; MIT, microtubule interacting and trafficking; MIM, MIT-interacting motif; ITC, isothermal titration calorimetry.

together with its cofactor LIP5 (Vta1) (12, 18, 29–32). Both VPS4 and LIP5 contain the MIT domain at their respective N termini, with VPS4 having one and LIP5 having two (23, 33–35). They are recruited to the membrane by binding to the exposed C-terminal MIMs of the membrane-bound ESCRT-III proteins. Binding of VPS4 and LIP5 by the ESCRT-III proteins also serves to regulate the VPS4 ATPase activity (22, 28). Hence, the MIT-MIM interaction plays an important role in determining the direction of information flow in the ESCRT machinery function. Here, we studied the structural basis that determines the specific binding mechanism in pairwise MIT-MIM interactions using the ESCRT-III protein IST1 as an example.

IST1 was initially identified as a yeast gene whose mutation affected multivesicular body biogenesis in vacuolar protein sorting (36, 37). Its mammalian ortholog was later found to be required for efficient abscission during cytokinesis (38). Biochemical analysis showed that IST1 binds to a number of MIT domain containing proteins, including VPS4, LIP5, and Spartin (38–40). Spartin is a multifunctional protein that is involved in localization or shaping of membrane compartments (41–44). The MIT-MIM-mediated interactions between IST1 and its binding partners are important for IST1 function as truncation of the C-terminal MIM sequence of IST1 led to defects in cytokinesis (24, 38). Interestingly, both Spartin and VPS4 are localized to the mid-body of dividing cells during cytokinesis, and this localization is dependent on their interaction with IST1 (24, 38, 39).

The MIT-MIM interaction has been shown to occur in one of the five binding modes, MIM1-MIM5, depending on where a MIM binds to on a MIT domain and the structure a MIM adopts when it interacts with a MIT domain (35, 45–51). For example, a peptide binds as a short α-helix to a groove formed between the second and third α-helices of the MIT domain in the MIM1 mode (45, 46), whereas it binds as an extended loop structure to a groove formed between the first and third α-helices of the MIT domain in the MIM2 mode (47). Peptides are often identified as potential MIMs based on their unique consensus binding sequences. They usually bind to the MIT domain via one of the five identified mechanisms.

IST1 displays some unique MIT domain binding features that have not been observed in other ESCRT-III proteins. Previous mutagenesis studies have suggested that IST1 can bind to the MIT domains of VPS4, LIP5, and Spartin utilizing different MIT-MIM binding mechanisms (24, 39). Given the importance of IST1 in recruiting VPS4 and Spartin to the mid-body of dividing cells during cytokinesis, we sought to understand the structural basis of the interaction between IST1 and these different MIT domain-containing proteins. To this end, we have determined the high resolution crystal structures of the IST1 C-terminal MIM in complex with the MIT domains of VPS4, LIP5, and Spartin, which showed that IST1 binds to VPS4 and LIP5 in the MIM1 mode but to Spartin in the MIM3 mode. Structural comparison showed that both MIT and MIM contribute to determine the specific binding mechanism in pairwise MIT-MIM interaction. Using a preliminary binding code derived from this analysis, we were able to convert CHMP2A, a protein that normally binds the MIT domain only in the MIM1 mode, into one that can also bind to the MIT domain of Spartin in the MIM3 mode.

EXPERIMENTAL PROCEDURES

Cloning, Expression, and Purification—Human $IST1^{312-335}$, $IST1^{290-335}$, $Spartin^{8-101}$, $VPS4B^{1-89}$, and $LIP5^{1-162}$ were expressed in *Escherichia coli* Rosetta (DE3) cells using a modified pET-28b vector with a SUMO protein tag inserted between a His_6 tag and the respective protein coding region. A tryptophan residue was appended to the C termini of IST1 fragments to facilitate spectral detection at 280 nm during purification. The addition of the residue did not affect IST1 interaction with various MIT domains as evidenced by the crystal structures as well as binding affinity measurement. Site-directed mutagenesis was performed using a standard PCR mutagenesis protocol (Stratagene). The codons used to introduce the point mutations for $IST1^{290-335}$ were F321A (TTT → GCG), L324A (CTT→ GCG), R327A (AGG → GCG), F328E (TTT → GAG), and L331A (CTG → GCG). The codons used to introduce the point mutations for $CHMP2A^{201-222}$ were D209F (GAT → CAG) and L216F (CTT → TTT).

All proteins were purified using a protocol as previously described (52). Briefly, bacterial cells were grown to mid-log phase in LB media at 37 °C and induced with 0.2 mM isopropyl β-D-1-thiogalactopyranoside for an additional 16–20 h at 16 °C. Harvested cells were lysed with sonication in buffer A (25 mM Tris (pH 8.0), 300 mM NaCl, 5 mM 2-mercaptoethanol, and 10 μg/ml (w/v) phenylmethylsulfonyl fluoride). Cell lysate was cleared by centrifugation, and supernatant was loaded onto a Ni^{2+}-nitrilotriacetic acid affinity column. Bound protein was washed with buffer A and eluted with buffer A supplemented with 250 mM imidazole. Fractions were pooled, and ULP1 protease was added to cleave off the His_6-SUMO tag. After dialysis against a buffer containing 50 mM Tris (pH 8.0) and 25 mM NaCl, the digested protein mixture was passed over a second Ni^{2+}-nitrilotriacetic acid column to remove undigested protein and the tag. For protein complexes used in structural studies, $IST1^{312-335}$ was mixed with $Spartin^{8-101}$, $VPS4B^{1-89}$, or $LIP5^{1-162}$ individually, and each complex was further purified by gel filtration chromatography on a Superdex75 column (GE Healthcare) equilibrated with a buffer containing 25 mM Tris (pH 7.3) and 100 mM NaCl.

Crystallization, Data Collection, and Structure Determination—All crystals were grown using the sitting drop vapor diffusion method. The $Spartin^{8-101}$-$IST1^{312-335}$ complex (20 mg/ml) was crystallized in 2.9 M sodium malonate (pH 6.0) at 4 °C, and crystals were cryo-protected in 3.0 M sodium malonate (pH 6.0). The $VPS4B^{1-89}$-$IST1^{312-335}$ complex (40 mg/ml) was crystallized in 2.58 M sodium malonate (pH 5.0) at 25 °C, and crystals were cryo-protected in 3.0 M sodium malonate (pH 5.0). The $LIP5^{1-162}$-$IST1^{312-335}$ complex (10 mg/ml) was crystallized in 30% (w/v) polyethylene glycol monomethyl ether 5000 (PEG5000MME), 0.1 M $(NH_4)_2SO_4$, and 0.1 M MES (pH 7.0) at 4 °C, and crystals were cryo-protected in 25% (w/v) PEG5000MME, 0.1 M $(NH_4)_2SO_4$, 0.1 M MES (pH 7.0), and 30% (v/v) ethylene glycol.

All diffraction data were collected at Advanced Photon Source LS-CAT 21-ID-F (Argonne National Laboratory). Crys-

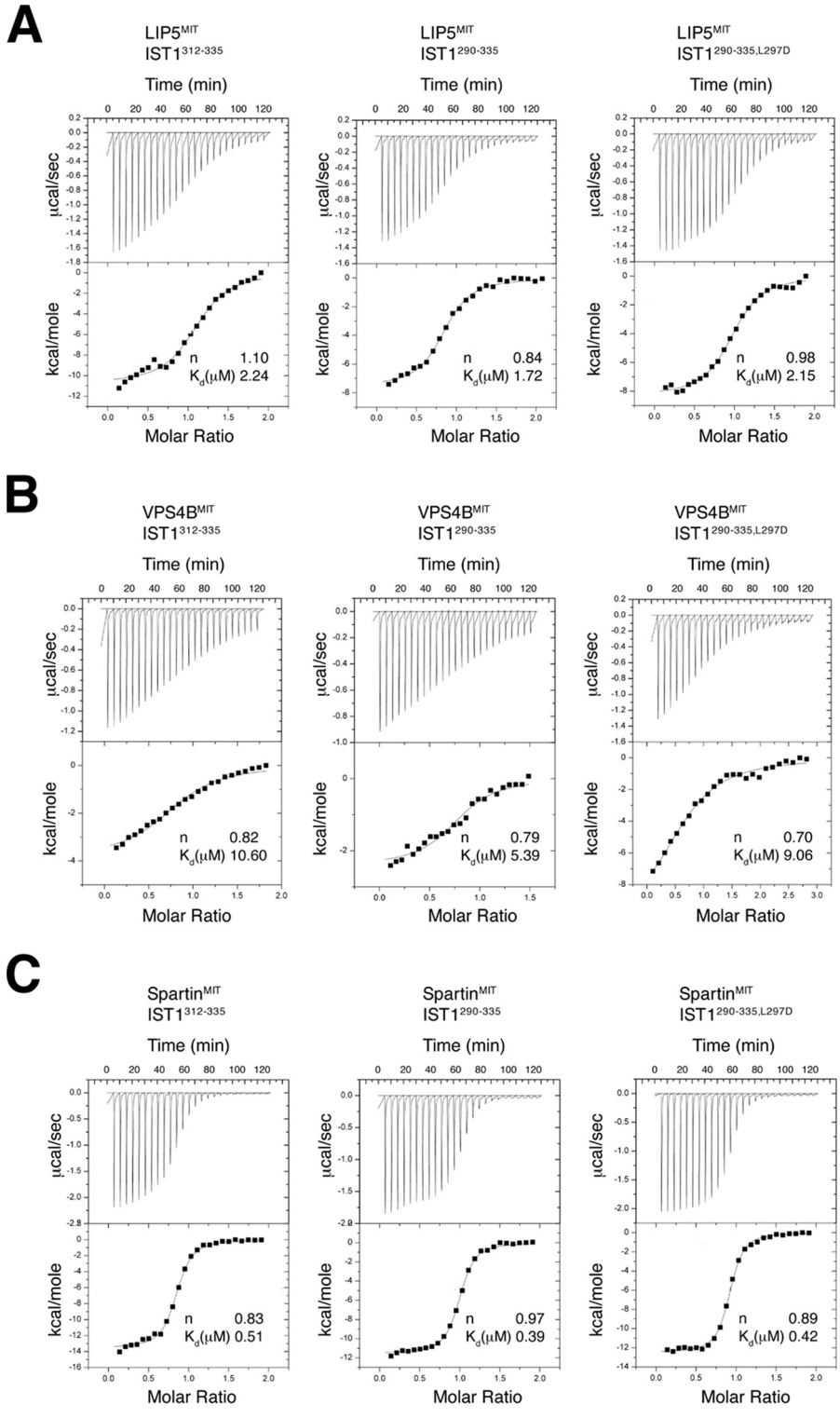

D

Binding affinities (K_d, µM) between IST1 and the MIT domains

	$IST1^{312-335}$	$IST1^{290-335}$	$IST1^{290-335, L297D}$
$LIP5^{MIT}$	2.24±0.50	1.72±0.14	2.15±0.26
$VPS4B^{MIT}$	10.6±1.8	5.39±1.32	9.06±2.88
$Spartin^{MIT}$	0.51±0.05	0.39±0.04	0.42±0.08

tals were cryo-cooled in liquid nitrogen during data collection. The Spartin$^{8-101}$-IST1$^{312-335}$ complex crystal diffracted to 1.8 Å and belonged to the space group of $P4_32_12$ with one complex in the asymmetric unit. The VPS4B$^{1-89}$-IST1$^{312-335}$ complex crystal diffracted to 2.5 Å and belonged to the space group of P622 with one complex in the asymmetric unit. The LIP5$^{1-162}$-IST1$^{312-335}$ complex crystal diffracted to 1.6 Å and belonged to the space group of $P2_12_12_1$ with one protein complex in the asymmetric unit. All data were processed using HKL2000 (HKL Research). The structures were solved by molecular replacement using the solution structures of the Spartin MIT domain (PDB entry 2DL1) and the VPS4B MIT domain (PDB entry 1WR0) and the crystal structure of LIP5 N-terminal domain (PDB entry 4TXP) as initial search models. The PHENIX software suite was used for structure determination and refinement (53). Model building was done with COOT (54). Data collection and structure refinement statistics are shown in Table 1.

Isothermal Titration Calorimetry—To measure the binding affinity between IST1 C-terminal fragments and various MIT domains, IST1 fragments were titrated against the MIT domains using a VP-ITC microcalorimeter (MicroCal) at 25 °C. Data were analyzed using the Origin 7 Software. All proteins were dialyzed against a buffer containing 25 mM HEPES (pH 7.5) and 50 mM NaCl, centrifuged to remove any particulate, and degassed before analysis. IST1 fragments were injected at 0.5 mM against 0.05 mM Spartin$^{8-101}$, 0.5 mM against 0.05 mM LIP5$^{1-162}$, and 0.85 mM against 0.09 mM VPS4B$^{1-89}$.

GST Pulldown Analysis—GST pulldown analysis was performed following standard protocols in a phosphate-buffered saline solution supplemented with 1 mM DTT and 0.1% (v/v) Tween 20 (52). GST alone, GST-tagged IST1$^{290-335}$ and its mutants, and GST-tagged CHMP2A$^{201-222}$ and its mutants were first immobilized on glutathione-agarose beads. Purified MIT domains were incubated with the protein-immobilized beads for 1 h at 4 °C. The beads were extensively washed with the buffer before bound proteins were analyzed on SDS-PAGE and visualized by either Coomassie staining or Western blotting.

Western Blotting—Proteins were separated by 15% SDS-PAGE and transferred onto nitrocellulose membrane. The membrane was first blocked by 5% (w/v) nonfat milk dissolved in the TBST buffer (50 mM Tris (pH 7.6), 150 mM NaCl, 0.05% (v/v) Tween 20) followed by incubation with mouse monoclonal antibody against a FLAG tag (1:5000 dilution, Sigma, catalogue number F3165) for 1 h. After three washes with the TBST buffer, the membrane was incubated with horseradish peroxidase-conjugated goat anti-mouse IgG (H+L) (1:5000 dilution, Anaspec, catalogue number 28173). After another three washes with the TBST buffer, the chemiluminescence reagent (Pierce ECL Plus Western blotting Substrate, Thermo) was added to the membrane. X-ray films (Premium Autoradiography Film, Denville Scientific) were exposed and developed to visualize the FLAG-tagged proteins.

RESULTS

IST1$^{312-335}$ Is Sufficient to Bind the MIT Domains of VPS4B, LIP5, and Spartin—Mutational and NMR spectroscopic studies have previously suggested that IST1 contains two potential MIM sequence motifs at its C terminus (24). Residues 312–335 resemble a peptide sequence that could bind in the MIM1 mode, and residues 290–308 resemble a peptide sequence that could bind in the MIM2 mode. These two sequence segments were hypothesized to wrap around the MIT domain, each binding to a different surface groove (24). With this model in mind, we initially attempted to crystallize various MIT-IST1 complexes using the IST1$^{290-335}$ fragment but were not met with success.

To improve our chance of obtaining diffraction-quality crystals, we set to reevaluate the energetic contributions of the two predicted MIMs of IST1 to MIT domain binding. Isothermal titration calorimetry (ITC) was used to determine the dissociation constants (K_d) for individual binding reactions between IST1 fragments and the MIT domains. We compared the binding behaviors of IST1$^{290-335}$ and IST1$^{312-335}$ to LIP5 MIT domain (LIP5^{MIT}, residues 1–162), VPS4B MIT domain (VPS4B^{MIT}, residues 1–89), and Spartin MIT domain (Spartin^{MIT}, residues 8–101). The results showed that there was no significant difference in binding affinity between the two IST1 fragments when they bound to any of the three MIT domains (Fig. 1). Furthermore, in the double MIM binding model of IST1, Leu-297 was predicted to be important for binding (24). However, L297D mutation of IST1 did not have a significant impact on the binding affinities between IST1$^{290-335}$ and any of the three MIT domains, suggesting that the residue is not required for MIT-IST1 interaction (Fig. 1). We, therefore, concluded that residues 290–311 of IST1 are dispensable for its interaction with the three MIT domains and that IST1$^{312-335}$ is a minimal fragment that is suitable for use in complex formation with all three MIT domains in the following structural studies.

Crystal Structures of the VPS4B-IST1 Complex and the LIP5-IST1 Complex—We first crystallized IST1$^{312-335}$ in complex with either VPS4B^{MIT} or LIP5^{MIT}. The VPS4B-IST1 complex structure was refined to 2.5 Å resolution (Table 1) with an R-factor/R_{free} of 22.5%/27.1%. The LIP5-IST1 complex structure was refined to a 1.6 Å resolution (Table 1) with an R-factor/R_{free} of 17.8%/20.1%. Some of the N-terminal residues (312–319 for both the VPS4B complex and the LIP5 complex) of IST1 were not visible in the electron density map and assumed to be disordered.

LIP5^{MIT} contains two tandem-linked MIT domains. Binding of IST1 occurs exclusively on the first domain. In both structures the binding site for the IST1 peptide is located on the surface groove formed by the second and third α-helices of the MIT domain (Fig. 2*A*). Most of the residues that form the peptide binding sites in the two structures occupy equivalent positions on the binding surface. For example, the binding site of VPS4B^{MIT} consists of side chains of Leu-31, Val-38, Leu-42,

FIGURE 1. **IST1$^{312-335}$ is a minimal MIT domain binding fragment of IST1.** *A–C*, binding affinities of LIP5^{MIT} (*A*), VPS4B^{MIT} (*B*), and Spartin^{MIT} (*C*) to various C-terminal fragments of IST1 and IST1 mutants were determined by ITC assay. Representative ITC enthalpy plots are shown. *D*, dissociation constants (K_d, μM) for various binding reactions calculated based on the ITC assay.

TABLE 1
Statistics for data collection and crystallographic refinement

Crystal	Spartin$^{8-101}$-IST1$^{312-335}$ complex	VPS4B$^{1-89}$-IST1$^{312-335}$ complex	LIP5$^{1-162}$-IST1$^{312-335}$ complex
Data collection			
Space group	$P4_32_12$	P622	$P2_12_12_1$
Unit cell parameters			
a, *b*, *c* (Å)	46.26, 46.26, 115.62	78.40, 78.40, 67.64	32.32, 65.58, 78.54
α, β, γ (°)	90, 90, 90	90, 90, 120	90, 90, 90
Molecules per asymmetric unit	1	1	1
Wavelength (Å)	0.9787	0.9787	0.9787
Resolution (Å)	1.8	2.5	1.6
Unique reflections[a]	12400	4455	22717
Redundancy	8.1 (8.4)	12.3 (12.7)	7.1 (7.0)
Completeness (%)	99.6 (100.0)	96.9 (98.2)	99.8 (99.4)
Average I/σ (I)	43.0 (4.0)	21.1 (6.4)	27.5 (4.1)
R_{merge}	0.081 (0.584)	0.112 (0.387)	0.060 (0.370)
Refinement			
Resolution range (Å)	29.61–1.79	33.82–2.50	33.69–1.60
R_{work} (%)	19.0	22.5	17.8
R_{free} (%)	22.1	27.1	20.1
Root mean square deviations			
Bond lengths (Å)	0.006	0.007	0.009
Bond angles (°)	0.942	0.997	1.283
B-factor average (A^2)	37.33	36.89	18.90
Number of solvent molecules	109	6	210
Ramachandran plot regions			
Most favored (%)	100.00	98.91	99.42
Allowed (%)	0	1.09	0.58
Outliers (%)	0	0	0
PDB entry	4U7I	4U7Y	4U7E

[a] Values in parentheses are for the specified high resolution bin.

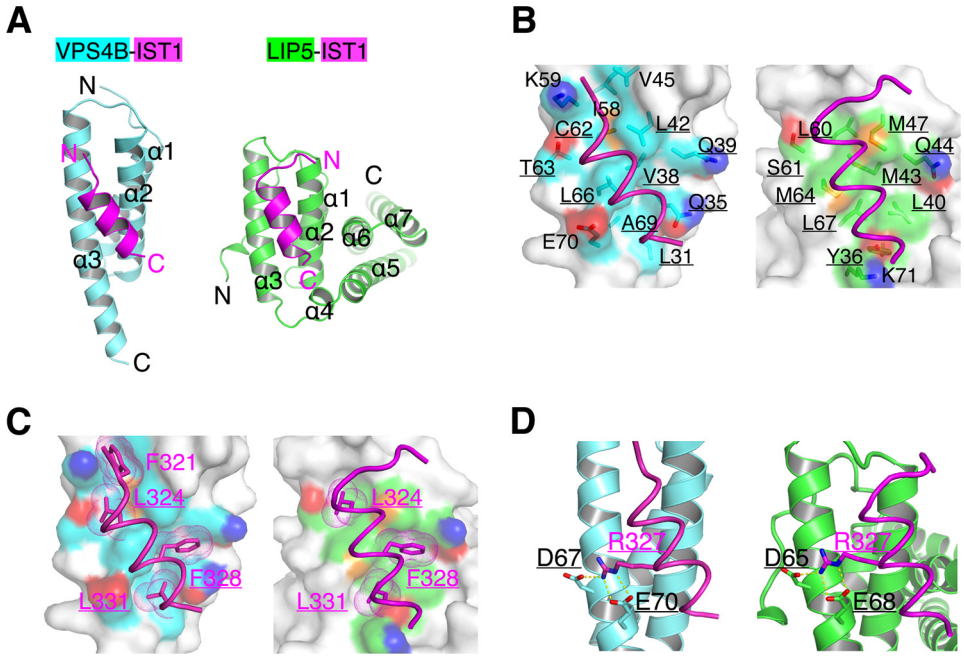

FIGURE 2. **Crystal structures of the VPS4B^{MIT}-IST1$^{312-335}$ complex (*left panel*) and the LIP5^{MIT}-IST1$^{312-335}$ complex (*right panel*).** *A*, ribbon representation. The helices in VPS4B^{MIT} and LIP5^{MIT} are labeled and colored in *cyan* and *green*, respectively. IST1$^{312-335}$ is colored in *magenta*. *B*, IST1 binding sites on the MIT domains. VPS4^{MIT} and LIP5^{MIT} are shown as semitransparent surface representations along with stick representations of side chains that contribute to van der Waals interactions. IST1$^{312-335}$ is shown as a *magenta coil*. *C*, hydrophobic IST1 residues that contribute to MIT domain binding. Side chains of hydrophobic IST1 residues that make direct contacts at the binding interfaces are shown as sticks along with dot representations of their van der Waals surfaces. *D*, polar interactions. Interacting residues are shown as stick models. Hydrogen bonds are denoted as *dashed lines*. Atoms in *B–D* are colored using the following scheme: carbon atoms of IST1$^{312-335}$, *magenta*; carbon atoms of VPS4^{MIT}, *cyan*; carbon atoms of LIP5^{MIT}, *green*; oxygen, *red*; nitrogen, *blue*; sulfur, *orange*. Surfaces are colored based on the underlying atoms. Labels for corresponding residues between the two structures are *underlined* and positioned at the same height.

Cyc-62, Leu-66, Ala-69, Gln-35, Gln-39 and Thr-63 (Fig. 2*B*). The equivalent positions in the LIP5^{MIT} structure are Tyr-36, Met-43, Met-47, Leu-60, Met-64, Leu-67, Leu-40, Gln-44, and Ser-61. Despite the differences in identity for some of the residues, they all engage in similar interactions with the IST1 residues. The bound IST1 peptide forms a three-turn α-helix. Four residues on the helix are responsible for nearly all of the interactions with the two MIT domains. Three hydrophobic residues, Leu-324, Phe-328, and Leu-331, bind to an overall hydrophobic surface (Fig. 2*C*). The fourth residue of IST1, Arg-327, forms salt bridges/hydrogen bonds with two acidic residues on the MIT domain, Asp-67 and Glu-70 (Asp-65 and Glu-68 for

LIP5) (Fig. 2*D*). The overall buried surface area at the interface is ~543 Å^2 and 545 Å^2 for the VPS4B-IST1 complex and the LIP5-IST1 complex, respectively. The mode of IST binding in these two structures is similar to what has been previously described as the MIM1 binding mode, as observed in the structures of the Vps4-Vps2 complex and the VPS4A-CHMP1A complex (45, 46). Therefore, IST1 binds to VPS4^{MIT} and LIP5^{NTD} in the MIM1 mode.

The Crystal Structure of the Spartin-IST1 Complex—We next crystallized IST1$^{312–335}$ in complex with Spartin^{MIT}. The structure was refined to 1.8 Å resolution (Table 1) with an R-factor/R_{free} of 19.0%/22.1%. As in the other two IST1 complex structures, residues 312–317 of the bound IST1 peptide were disordered.

The most significant difference in IST1 binding to Spartin as compared with VPS4B and LIP5 is that IST1 binds to a different surface groove of the MIT domain. The binding site, instead of being located on the surface groove between the second and third α-helices, is located on the surface groove between the first and third α-helices of the MIT domain (Fig. 3*A*). A similar mode of interaction has been previously observed in the structure of the microtubule severing AAA-ATPase Spastin MIT domain in complex with ESCRT-III protein CHMP1B (48). This type of interaction where a peptide binds to a MIT domain as a helix on the surface groove between the first and third α-helices has been referred to as the MIM3 binding mode. Therefore, the C-terminal peptide sequence of IST1 can bind to different MIT domains either in the MIM1 or in the MIM3 mode.

Residues that line the binding groove of Spartin^{MIT} are mostly hydrophobic, but a few polar side chains are also present. These include Tyr-20, Phe-24, Val-27, Asn-28, Leu-31, Asp-34, Asn-32, and Glu-35 of helix 1 and Lys-80, Thr-84, Asn-87, Val-88, and Arg-91 of helix 3 (Fig. 3*B*). Interestingly, there are also two residues from helix 2, Leu-53 and Tyr-46, lining the floor of the binding groove. The bound IST1 peptide forms a three-turn α-helix with a total of seven residues making direct contacts with the Spartin MIT domain. At the core of the interface, hydrophobic residues Ile-319, Phe-321, Leu-324, Phe-328, and Leu-331 of IST1 make van der Waals contacts with the hydrophobic surface of the MIT domain (Fig. 3*C*). In particular, two bulky aromatic side chains Phe-321 and Phe-328 fit snugly into two deep surface pockets. At the periphery, Asp-322 and Arg-327 of IST1 participate in specific hydrogen bond and salt bridge interactions with the Spartin residues. Arg-327 forms a total of four hydrogen bonds with Glu-35, Asn-28, and Asn-32 from Spartin (Fig. 3*D*). Compared with the MIM1 binding surface on VPS4B or LIP5, the MIM3 binding surface on Spartin is much more extensive with some deep binding pockets. The overall buried surface area at the interface is ~740 Å^2.

Comparison with the Spastin-CHMP1B Complex Structure—As noted above, the MIM3 binding mode has been previously observed in the crystal structure of the Spastin-CHMP1B complex (48). Comparison between the two structures revealed interesting features unique to the MIM3 binding mode. Although CHMP1B binds to Spastin as a much longer six-turn α-helix, the C-terminal three turns fits into a hydrophobic groove on the surface of the Spastin MIT domain in a nearly

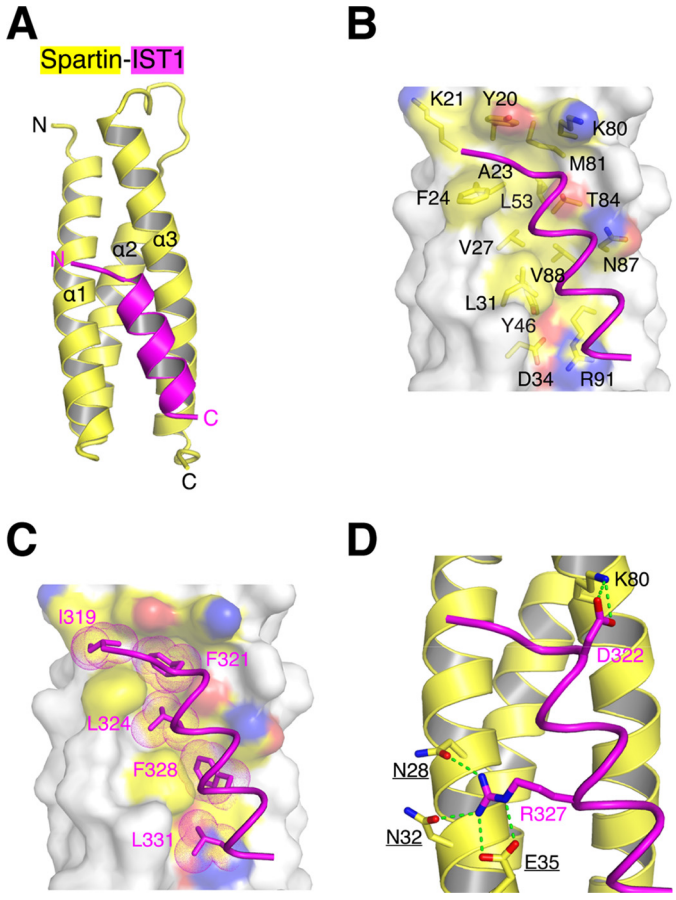

FIGURE 3. **Crystal structure of the Spartin^{MIT}-IST1$^{312–335}$ complex.** *A*, ribbon representation. The helices in Spartin^{MIT} are labeled and colored in *yellow*. IST1$^{312–335}$ is colored in *magenta*. *B*, IST1 binding site on the MIT domain. Spartin^{MIT} is shown as a semi-transparent surface representation along with stick representation of side chains that contribute to van der Waals interactions. IST1$^{312–335}$ is shown as a *magenta coil*. *C*, hydrophobic IST1 residues that contribute to MIT domain binding. Side chains of hydrophobic IST1 residues that make direct contacts at the binding interface are shown as sticks along with *dot representation* of their van der Waals surfaces. *D*, polar interactions. Interacting residues are shown as stick models. Hydrogen bonds are denoted as *dashed lines*. Atoms and surfaces in *B–D* are colored using the same scheme as in Fig. 2 with the exception of carbon atoms of Spartin^{MIT}, which is colored *yellow*.

identical fashion as IST1 to Spartin (Fig. 4*A*). Six residues on these three helical turns make critical contribution to Spastin binding. Asp-186, Leu-188, Arg-191, Leu-192, and Leu-195 of CHMP1B are structurally analogous to Asp-322, Leu-324, Arg-327, Phe-328, and Leu-331 of IST1. The binding pockets for these side chains are formed mostly with conserved residues on the MIT domain surface (Fig. 4*C*). Hence, the binding modes for the C-terminal three helical turns of IST1 and CHMP1B are similar in the two cases. Based on the structural alignment, Gln-185 of CHMP1B is at a similar position as Phe-321 of IST1. Although they are both critical for high affinity MIM3 binding, their modes of interaction are quite different. Phe-321 of IST1 inserts itself into a deep hydrophobic pocket on Spartin, whereas Gln-185 of CHMP1B is involved in an extensive hydrogen bond network with His-120 and Asn-184 of Spastin (Fig. 4*B*).

Although the IST1 peptide used in our study is long enough to form a six-turn α-helix, only a three-turn α-helix was observed in the structure. A close examination of the Spartin-

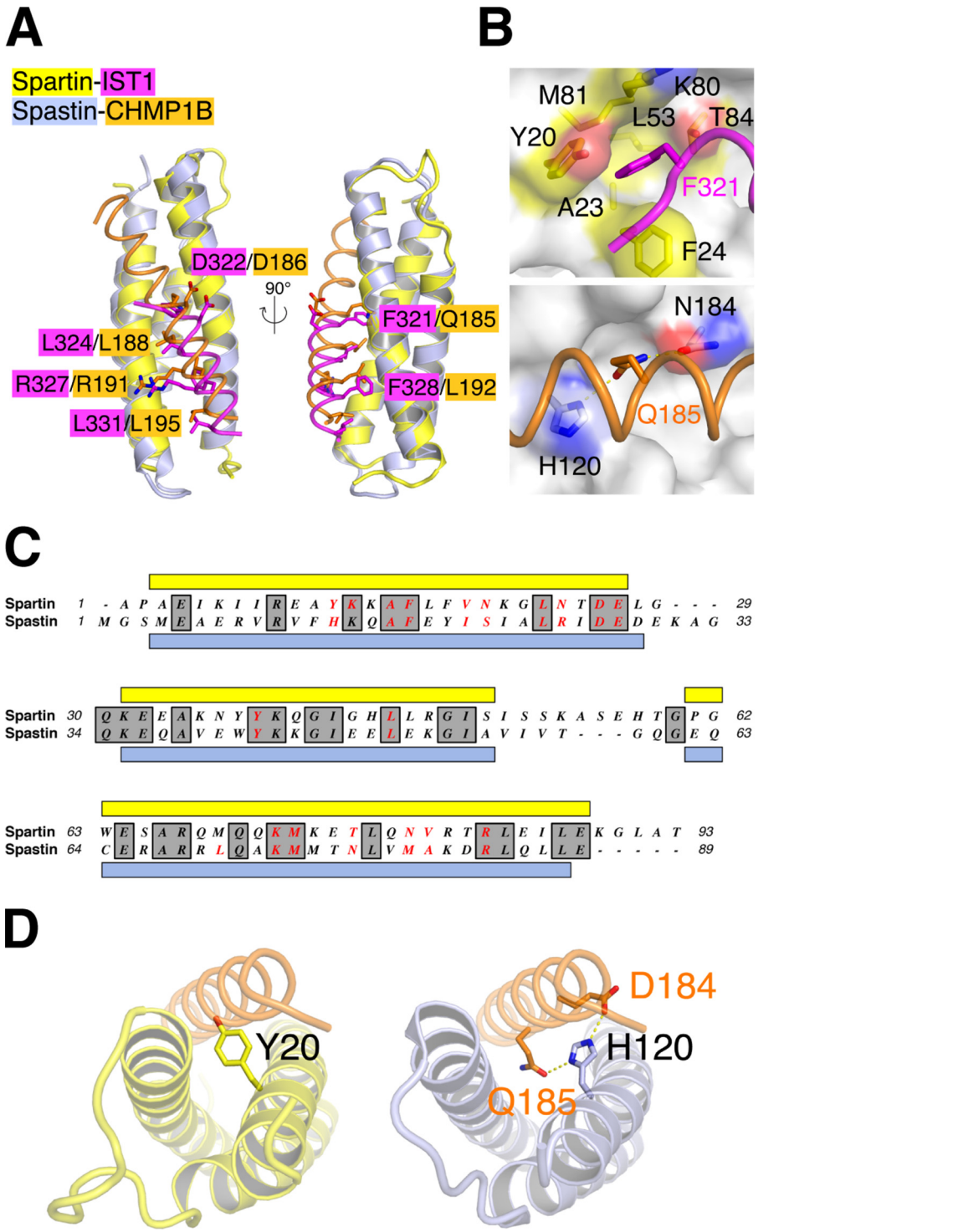

FIGURE 4. **Comparison between the two MIT-MIM3 complex structures.** *A*, structural alignment of the Spartin^{MIT}-IST1 complex and the Spastin^{MIT}-CHMP1B complex shown in two orthogonal views. Spartin^{MIT} and Spastin^{MIT} are *yellow* and *light blue ribbons*; IST1 and CHMP1B are *magenta* and *orange coils*. Six IST1 residues that make critical contribution to Spartin binding are shown as sticks along with their counterparts in CHMP1B. *B*, zoom-in views of the binding pockets for F321 (IST1, *top*) and Q185 (CHMP1B, *bottom*). The corresponding MIT domains are shown as semi-transparent surface representations along with stick representation of side chains that contribute to specific interactions. *C*, sequence alignment of Spartin^{MIT} and Spastin^{MIT}. Secondary structures (helices) are shown as *rectangles above* (Spartin) or *below* (Spastin) the sequences. Conserved residues are *shaded* and *boxed*. Spartin and Spastin residues involved in binding to the six residues shown in *A* are colored *red*. *D*, Tyr-20 of Spartin^{MIT} prevents IST1 from binding as a long helix. *Left*, a composite structure model of Spartin^{MIT}-CHMP1B showing the potential steric clash between Tyr-20 and a long helix. *Right*, crystal structure of the Spastin^{MIT}-CHMP1B complex showing how the long helix of CHMP1B is accommodated by Spastin^{MIT}. Atoms in *A*, *B*, and *D* are colored using the following scheme: carbon atoms of IST1, *magenta*; carbon atoms of Spartin^{MIT}, *yellow*; carbon atoms of CHMP1B, *orange*; carbon atoms of Spastin^{MIT}, *light blue*; oxygen, *red*; nitrogen, *blue*.

IST1 structure offered a plausible explanation. N-terminal to Phe-321, the bulky side chain of Tyr-20 of Spartin sticks out on the protein surface (Fig. 4*D*). If the IST1 peptide were to form a longer helix, it would clash directly with Tyr-20. Instead, the N-terminal portion of the IST1 peptide breaks away from the helical trajectory. This conformation appears to be further stabilized by the interaction of Ile-319 with Spartin. Consequently, the N terminus of the IST1 peptide extends away from the MIT domain and adopts a flexible conformation not observable in the current crystal structure. The structural equivalent of Tyr-20 in Spastin is His-120, which has moved out of the helical path due to its interaction with Gln-185 of CHMP1B. Therefore, CHMP1B is able to bind to Spastin as a much longer helix.

The Role of Phe-321 of IST1 in Binding to Spartin—Many ESCRT-III proteins contain C-terminal sequences that can interact the MIT domain in the MIM1 binding mode. Yet, only two of them (IST1 and CHMP1B) have been observed to also interact the MIT domain in the MIM3 binding mode (45, 47, 48). To gain further insight into the mechanism of selectivity for an ESCRT-III protein to bind specific MIT domains either in the MIM1 or in the MIM3 mode, we compared the MIT-MIM interfaces in the three determined MIT-IST1 complex structures.

Five residues of IST1 appear to be important for the complex formation in the three structures. Common to all three are Leu-324, Phe-328, Arg-327, and Leu-331. The three hydrophobic residues bind to hydrophobic pockets on the surface of the respective MIT domain, and Arg-327 is involved in multiple hydrogen bond interactions. Among them, the binding pocket for Phe-328 appears to be deeper in the Spartin MIT domain than in the other two MIT domains. On the other hand, there is a significant difference in the way Phe-321 interacts with the three MIT domains due to the distinct conformation the IST1 peptide adopts in the three structures (Fig. 5*A*). In the LIP5-IST1 complex structure, Phe-321 is located in a loop region of the peptide and points away from the interface (Fig. 5*B*). It does not make any contact with LIP5. Phe-321 interacts with the other two MIT domains in different manners. In the Spartin-IST1 complex structure, Phe-321 is deeply buried in a hydrophobic pocket and interacts with Phe24, Tyr-20, and Thr-84 (Fig. 5*D*). In the VPS4B-IST1 complex structure, the phenylalanine side chain interacts with a much shallower binding pocket formed by Val-45 and the aliphatic portion of the Arg-59 side chain (Fig. 5*C*).

To evaluate the energetic contribution of individual IST1 residues to all three binding interactions, point mutations were introduced at selective sites on IST1, and mutant proteins were examined for their binding interactions with the three MIT domains. We chose to use $IST1^{290-335}$ in our binding analysis because full-length IST1 was unstable and degraded rapidly. Wild-type $IST^{290-335}$ displayed strong binding to all three MIT domains. F321A had little impact on binding to LIP5 but displayed dramatically reduced binding to Spartin in both ITC and GST pulldown analyses (Fig. 6, *A* and *B*). GST pulldown analysis also showed that F321A retained partial binding to VPS4B, but an accurate determination of K_d could not be made by ITC. These results were consistent with the structural observation where Phe-321 displayed different degrees of engagement with

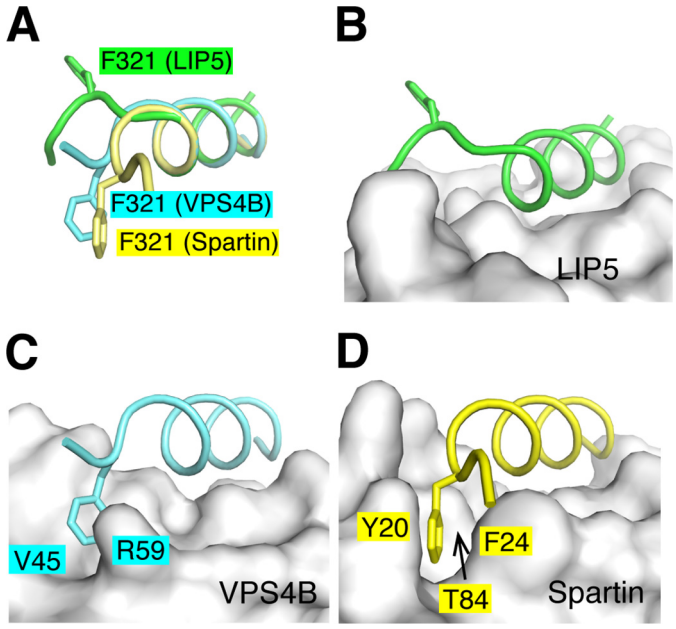

FIGURE 5. **Phe-321 of IST1 adopts different conformation in the three complex structures.** *A*, structural alignment of $IST1^{312-335}$ as observed in the three complex structures: in $Spartin^{MIT}$, *yellow*; in $VPS4B^{MIT}$, *blue*; and in $LIP5^{MIT}$, *green*. Phe-321 side chains are shown as stick models. *B–D*, the binding pockets of Phe-321 in the three complex structures: $LIP5^{MIT}$ (*B*), $VPS4B^{MIT}$ (*C*), and $Spartin^{MIT}$ (*D*). MIT domains are shown as semi-transparent surface representations. Residues within each MIT domain that contribute to Phe-321 binding are labeled. Note that the binding pocket of Phe-321 is significantly deeper in $Spartin^{MIT}$ than in $VPS4B^{MIT}$.

the three MIT domains. Leu-324, Phe-328, Leu-331, and Arg-327, on the other hand, are engaged in similar degrees of binding in all three MIT domain complex structures. Not surprisingly, L324A, F328E, and L331A abolished or dramatically reduced binding to all three MIT domains (Fig. 6, *C*, *D*, and *E*). R327A also displayed a significant decrease in binding to all three MIT domains (data not shown).

Engineering a MIM1 to Bind Spartin as a MIM3—Given the importance of Phe-321 in supporting IST1 binding to the Spartin MIT domain in the MIM3 binding mode, we wondered whether adding a phenylalanine residue to an ESCRT-III protein that normally only binds in the MIM1 mode would provide the protein the additional ability to bind in the MIM3 mode. The ESCRT-III protein CHMP2A contains the MIM1 consensus sequence of (D/E)*XX*L*XX*RL*XX*L(K/R) (*X* indicates any residue) (Fig. 7*A*). The crystal structure of Vps2 (the yeast ortholog of human CHMP2A) in complex with the MIT domain of Vps4 showed that the protein binds to Vps4 in the MIM1 mode (46). Furthermore, CHMP2A does not bind to the MIT domain of Spartin (39).

We first introduced a D209F mutation (the equivalent position of Phe-321) to the CHMP2A sequence. However, GST pulldown analysis followed by Western blotting detection showed that $CHMP2A^{201-222,\ D209F}$ did not bind to the Spartin MIT domain. We recalled that the second hydrophobic residue of the MIM1 consensus sequence in IST1 is a bulky phenylalanine that binds to a deep surface pocket on the Spartin MIT domain. In other MIM1 containing ESCRT-III proteins including CHMP2A, this position is usually occupied by a leucine that may not provide sufficient binding energy for a stable MIM3

A

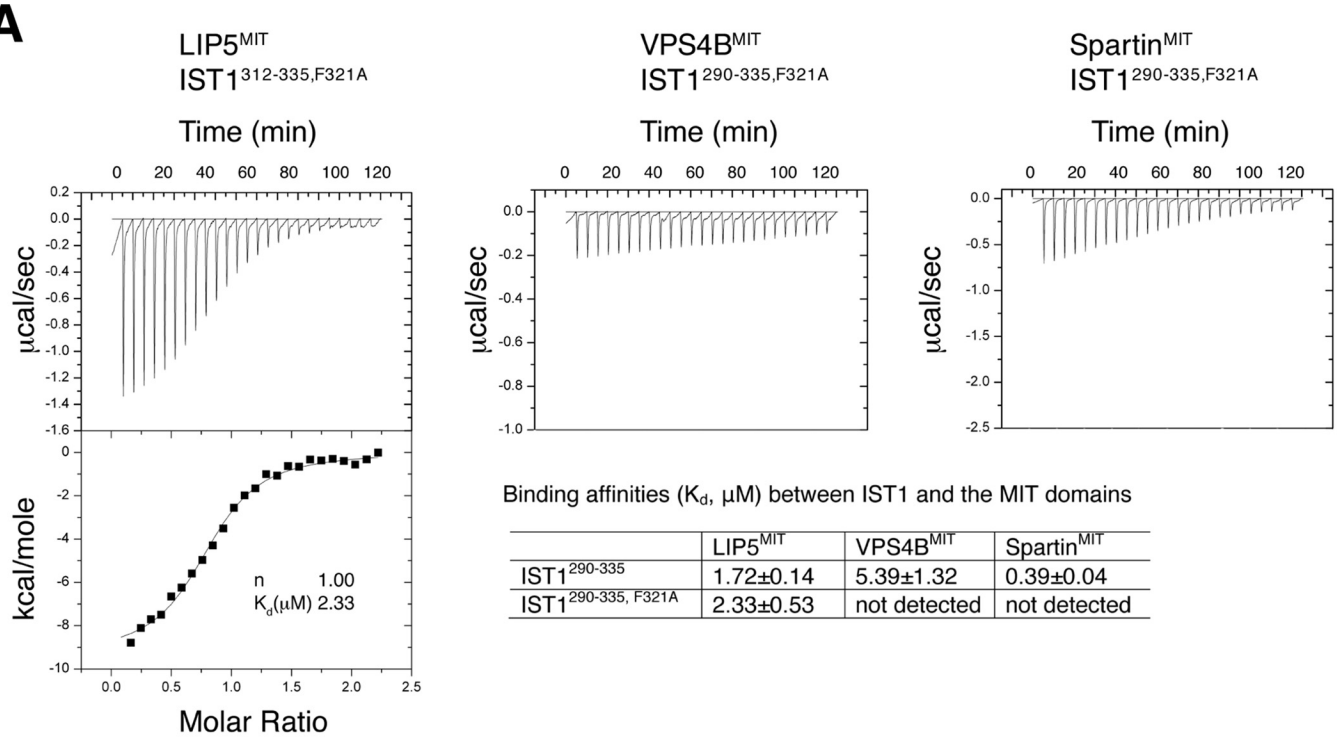

Binding affinities (K_d, µM) between IST1 and the MIT domains

	$LIP5^{MIT}$	$VPS4B^{MIT}$	$Spartin^{MIT}$
$IST1^{290-335}$	1.72±0.14	5.39±1.32	0.39±0.04
$IST1^{290-335, F321A}$	2.33±0.53	not detected	not detected

B

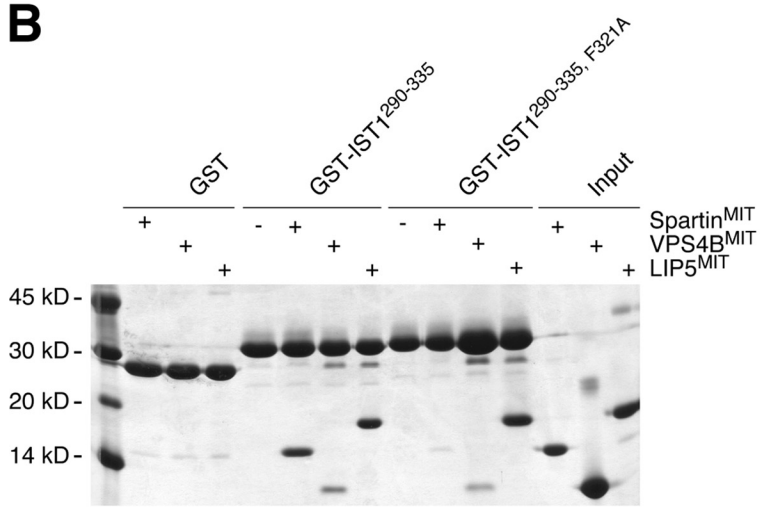

C

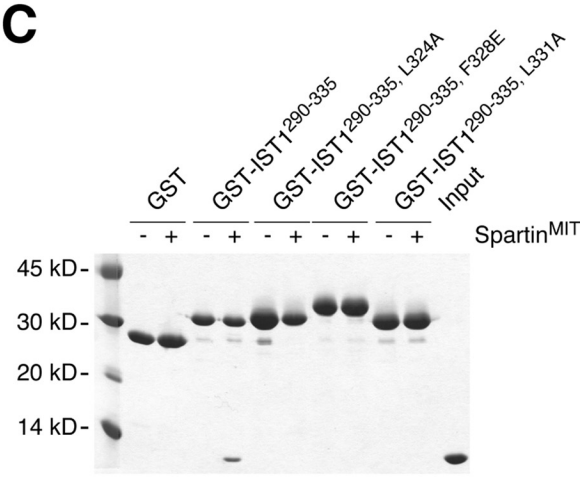

D

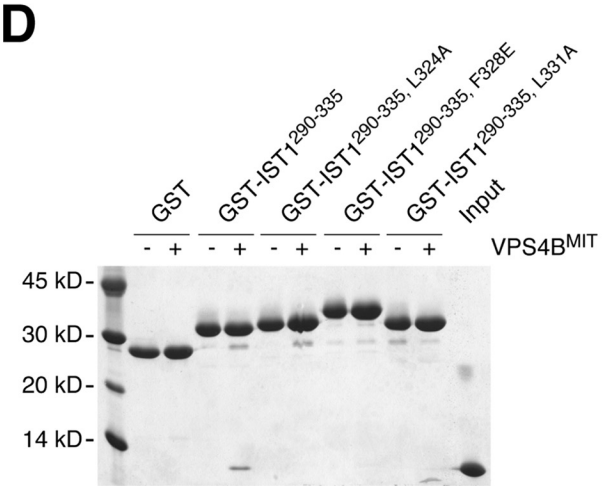

E

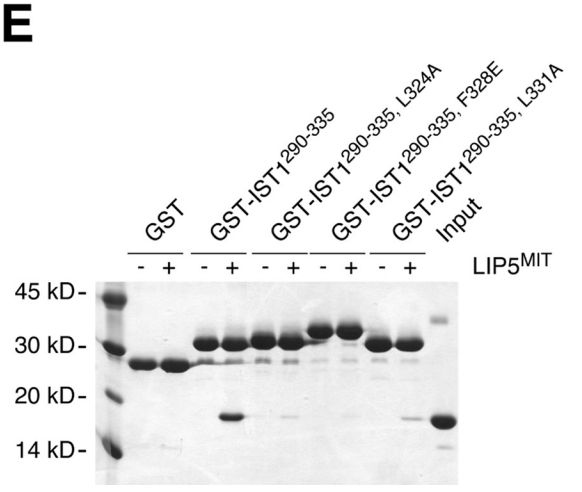

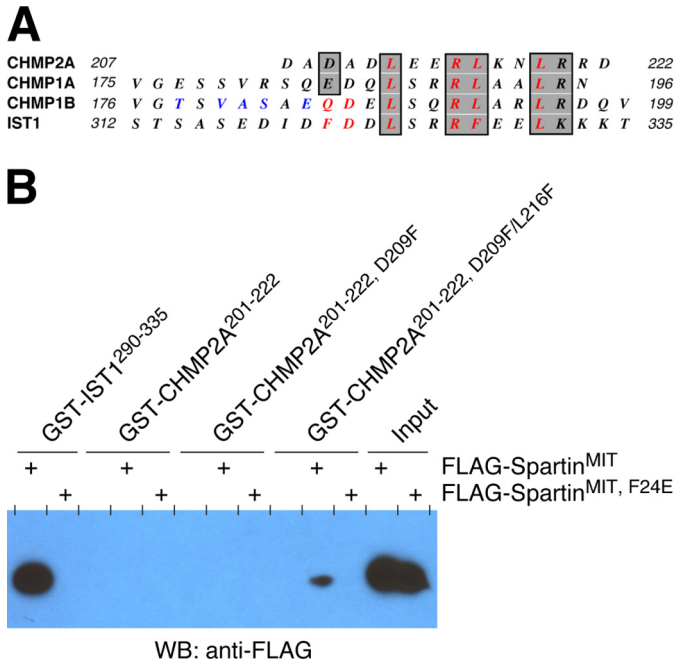

FIGURE 7. **Mutant CHMP2A can bind to Spartin as a MIM3.** *A*, sequence alignment of the C-terminal MIM motifs of CHMP2A, CHMP1A, CHMP1B, and IST1. Core residues of MIM1 are *shaded* and *boxed*. Core residues of MIM3 are colored in *red*. Other residues that are important for Spastin^{MIT}-CHMP1B^{MIM} interaction are colored in *blue*. *B*, GST, GST-CHMP2A$^{201–222}$, GST-CHMP2A$^{201–222, D209F}$, and GST-CHMP2A$^{201–222, D209F/L216F}$ were used to pull down FLAG-Spartin^{MIT} or FLAG-Spartin$^{MIT, F24E}$. Anti-FLAG antibody was used to detect the binding of FLAG-Spartin^{MIT} or FLAG-Spartin$^{MIT, F24E}$. Only GST-CHMP2A$^{201–222, D209F/L216F}$ can bind to Spartin^{MIT}. *WB*, Western blot.

interaction (Fig. 7*A*). Hence, we introduced a second mutation to the CHMP2A sequence. Indeed, the double mutant, CHMP2A$^{201–222, D209F/L216F}$, showed binding to the Spartin MIT domain (Fig. 7*B*). To determine where the mutant CHMP2A fragment binds on Spartin, we tested its binding to Spartin$^{MIT, F24E}$. Phe-24 is located on the surface groove between helices α1 and α3 of the Spartin MIT domain and is critical for a peptide to bind in the MIM3 mode. No binding was observed between CHMP2A$^{201–222, D209F/L216F}$ and Spartin$^{MIT, F24E}$. This result strongly suggested that the mutant CHMP2A bound to the Spartin MIT domain in the MIM3 mode. Interestingly, it retained its ability to bind to the VPS4B MIT domain in the MIM1 mode (data not shown). Therefore, the sequence of F*XXLXX*R*FXX*L appears to be sufficient for binding to the VPS4B MIT domain in the MIM1 mode as well as to the Spartin MIT domain in the MIM3 mode.

DISCUSSION

The ESCRT-III proteins play critical roles in the ESCRT machinery. Not only has their polymerization and subsequent membrane association been demonstrated to be directly linked to producing membrane curvature and generating force for vesicle scission, but they are also responsible for recruiting proteins, including ATPases and deubiquitinases, to the site of action. In addition, there are at least three ESCRT-III like proteins whose main function involves regulation of the ESCRT machinery. Central to the function of the ESCRT-III proteins is their binding to a unique protein-protein interaction domain called the MIT domain. Interactions between the MIT domain and the ESCRT-III proteins have been shown to be important for the proper progression of the cellular processes that require the ESCRT machinery. Therefore, understanding the structural basis of MIT domain interaction is key to understanding the molecular mechanism underlying the ESCRT-III function.

The MIT domain contains an up-and-down triple helix bundle fold and recognizes MIM peptide sequences located at or near the C termini of the ESCRT-III proteins (11). Despite the simple structural fold of the MIT domain, its interaction with MIM is by no means simple. A single MIT domain can utilize different surface grooves to bind different MIMs, with bound peptides adopting different structural conformations. Conversely, a single MIM can also bind to different MIT domains using different binding mechanisms. To date, at least five different modes of MIT-MIM interaction have been described structurally. Although these structures offered a glimpse into the complicated nature of MIT-MIM interaction, we are still far from having a code of binding that can be used to reliably predict how a specific pair of MIT-MIM might interact. In the current study we have determined the crystal structures of three new MIT-MIM complexes with the same MIM peptide sequence from IST1. This enabled us for the first time to directly compare how one MIM can engage in different types of MIT-MIM interactions.

Based on the results from previous structural studies, the consensus sequence for a peptide to bind in the MIM1 mode has been defined as (D/E)*XXLXX*R*LXX*L(K/R). The ESCRT-III proteins that are predicted to contain a MIM1 binding sequence include CHMP1, CHMP2, CHMP3, and IST1. The crystal structures of the VPS4B-IST1 complex and the LIP5-IST1 complex showed that IST1 binds to these MIT domains in the MIM1 mode. Only four residues of IST1, Leu-324, Arg-327, Phe-328, and Leu-331, are involved in direct binding in both structures. Therefore, it seems that the core sequence requirement for a peptide to bind in the MIM1 mode can be reduced to L*XX*RΦ*XX*L (Φ stands for hydrophobic residues). The second hydrophobic residue in this sequence is often a leucine but in IST1 is occupied by a phenylalanine residue that binds to a deep surface pocket. It is possible that the more extensive interface provided by the bulky side chain offsets the requirement of the two polar interactions at the end of the original MIM1 consensus sequence.

IST1 was originally proposed to bind to the VPS4 MIT domain using two sequence segments, one in the MIM1 mode and the other in the MIM2 mode (24). During our study, we discovered that the predicted MIM2 segment was dispensable for IST1 to form stable complexes with the three tested MIT domains. Several lines of evidence supported our conclusion.

FIGURE 6. **Contributions of individual IST1 residues to MIM1 and MIM3 binding.** *A*, binding affinities of LIP5^{MIT}, VPS4B^{MIT}, and Spartin^{MIT} to IST1$^{290–335, F321A}$ were determined by ITC assay. Representative ITC enthalpy plots are shown. *B*, GST, GST-IST1$^{290–335}$ and GST-IST1$^{290–335, F321A}$ were used to pull down Spartin^{MIT}, VPS4B^{MIT}, and LIP5^{MIT}. *C–E*, GST, GST-IST1$^{312–335}$, GST-IST1$^{312–335, L324A}$, GST-IST1$^{312–335, F328E}$, and IST1$^{312–335, L331A}$ were used to pull down Spartin^{MIT} (*C*), VPS4B^{MIT} (*D*), and LIP5^{MIT} (*E*). Proteins retained on the beads were analyzed by SDS-PAGE and visualized by Coomassie staining.

First, there is no significant difference in binding affinity between a longer IST1 fragment with both MIM segments and a shorter one with only the MIM1 segment. Second, mutation of a consensus leucine residue that is required in the canonical MIM2 binding mode has no impact on MIT-IST1 interaction. Finally, the crystal structure of the LIP5-IST1 complex showed that the potential MIM2 binding site on the first MIT domain of LIP5 (which binds IST1) is engaged in an intramolecular interaction and thus not available for binding the putative MIM2 segment of IST1. Taken together, although we cannot rule out the possibility of minor contacts involving the sequence upstream of residues 312–335, it is likely that the C-terminal 24 residues of IST1 provide nearly all of the binding energy in engaging the MIT domains.

The MIM3 binding mode has only been previously observed in the Spastin-CHMP1B complex structure where CHMP1B binds as a six-turn α-helix to the surface groove formed by the first and third helices of the MIT domain. This interaction was observed to be of higher affinity than the MIM1 binding mode. The difference was attributed to the fact that the MIM peptide binds as a longer helix and its associated larger binding interface. In the current study we showed that a longer helix is not a structural requirement for IST1 to engage in the high affinity MIM3 interaction with Spartin. In fact, although the IST1 fragment used in crystallization is long enough to form a six turn α-helix, the surface feature of Spartin is not conducible for extended IST1 binding. How does the shorter IST1 helix achieve high affinity binding? Structural comparison between the two MIT-MIM3 complex structures offered some clues. Six MIT binding residues on the C-terminal portion of CHMP1B have corresponding residues in IST1. Two of them have different sequence identities. Both Phe-321 and Phe-328 of IST1 are buried deeply in their respective binding pockets. They likely provide significant binding energy to allow a shorter IST1 helix to bind Spartin tightly. In CHMP1B, these two residues are replaced by glutamine and leucine, respectively. Although both are still involved in MIT domain interaction, they are unlikely to provide a similar level of binding energy. Therefore, the C-terminal half of CHMP1B alone is not sufficient and requires additional contacts at the N-terminal half for high affinity binding.

The above observation suggests that structural features in both MIT and MIM are important in determining the specific binding mechanism in pairwise interaction. As we have seen in the two MIT-MIM3 complex structures, the surfaces where the IST1 helix and the C-terminal half of the CHMP1B helix bind are very similar. The deep binding pockets at these locations enable the ESCRT-III proteins to bind both Spartin and Spastin in the MIM3 mode. Yet, for a specific ESCRT-III protein to bind, certain sequence requirements must be satisfied as we have seen in the case of IST1 and CHMP1B. In the presence of the two bulky phenylalanine residues, it is likely that a three-turn helix is sufficient for IST1 to bind to both Spartin and Spastin in the MIM3 mode. On the other hand, binding of CHMP1B requires the peptide to adopt a longer six-turn helix due to the lack of sufficient binding energy from the C-terminal half alone. This binding is possible with Spastin but not with Spartin due to steric clashes with surface features on the Spartin MIT domain. This explains why IST1 can bind to both Spartin and Spastin, whereas CHMP1B only binds to Spastin.

FIGURE 8. **Alignment of the C-terminal MIM sequences of IST1 from selective genomes.** The *top block* contains IST1 from fungi. The *bottom block* contains IST1 from high eukaryotes. Residues that are important for MIT domain binding are indicated by *triangles*.

Most of the ESCRT-III proteins that contain a C-terminal consensus MIM1 sequence fragment do not contain phenylalanine in the two corresponding positions and, therefore, cannot bind the Spartin MIT domain in the MIM3 mode. However, by introducing two phenylalanine residues into the C-terminal sequence of CHMP2A, we enabled the ESCRT-III protein to bind the Spartin MIT domain in the MIM3 mode. The role of the two phenylalanine residues was further hinted by examining evolutionary data. Although IST1 orthologs exist in all eukaryotic genomes, there is no Spartin or Spastin ortholog in fungal genomes. Phylogenetic analysis showed that there is a strong correlation between the presence of Spartin or Spastin gene in a given genome and the conservation of the two phenylalanine residues in the corresponding IST1 sequence (Fig. 8). These data suggest that the early function of IST1 was likely to bind the MIT domain only in the MIM1 mode. As Spartin and Spastin genes were later acquired in the genomes of high eukaryotes, IST1 also evolved to have the additional ability to bind in the MIM3 mode.

IST1 is required for recruiting both VPS4 and Spartin to the mid-body of dividing cells. The ability of IST1 to bind different MIT domains either in the MIM1 or in the MIM3 mode is thus biologically important. How IST1 partitions binding among various MIT domains in the cell is an interesting question in addressing the molecular mechanism of the ESCRT machinery. Given that IST1 is the only ESCRT-III protein recognized by Spartin and the binding affinity between the two proteins is much higher than that between IST1 and VPS4, it is tempting to speculate that IST1-Spartin interaction predominates in the cell. Our results have so far provided a preliminary code that can be used to selectively study specific pair of MIT-IST1 interaction through site-directed mutagenesis, which will provide

new mechanistic insights with regard to the molecular interaction between IST1, VPS4, and Spartin in cytokinesis and other biological processes.

Acknowledgments—We thank the staff at the Advanced Photon Source Sector 21 (21-ID-F) for access and help with data collection. Use of the Advanced Photon Source, an Office of Science User Facility operated for the United States Department of Energy (DOE) Office of Science by Argonne National Laboratory, was supported by the United States DOE under Contract DE-AC02-06CH11357. Use of the LS-CAT Sector 21 was supported by the Michigan Economic Development Corp. and the Michigan Technology Tri-Corridor (Grant 085P1000817). We thank C. Vild and Y. Li for helpful discussion and K. Chinnaswamy and B. Wan for access and help for ITC experiments.

REFERENCES

1. Hurley, J. H., and Hanson, P. I. (2010) Membrane budding and scission by the ESCRT machinery: it's all in the neck. *Nat. Rev. Mol. Cell Biol.* **11,** 556–566
2. McCullough, J., Colf, L. A., and Sundquist, W. I. (2013) Membrane fission reactions of the mammalian ESCRT pathway. *Annu. Rev. Biochem.* **82,** 663–692
3. Henne, W. M., Buchkovich, N. J., and Emr, S. D. (2011) The ESCRT pathway. *Dev. Cell* **21,** 77–91
4. Gruenberg, J., and Stenmark, H. (2004) The biogenesis of multivesicular endosomes. *Nat. Rev. Mol. Cell Biol.* **5,** 317–323
5. Katzmann, D. J., Odorizzi, G., and Emr, S. D. (2002) Receptor downregulation and multivesicular-body sorting. *Nat. Rev. Mol. Cell Biol.* **3,** 893–905
6. Morita, E., and Sundquist, W. I. (2004) Retrovirus budding. *Annu. Rev. Cell Dev. Biol.* **20,** 395–425
7. Carlton, J. G., and Martin-Serrano, J. (2007) Parallels between cytokinesis and retroviral budding: a role for the ESCRT machinery. *Science* **316,** 1908–1912
8. Jimenez, A. J., Maiuri, P., Lafaurie-Janvore, J., Divoux, S., Piel, M., and Perez, F. (2014) ESCRT machinery is required for plasma membrane repair. *Science* **343,** 1247136
9. Williams, R. L., and Urbé, S. (2007) The emerging shape of the ESCRT machinery. *Nat. Rev. Mol. Cell Biol.* **8,** 355–368
10. Hurley, J. H., and Emr, S. D. (2006) The ESCRT complexes: structure and mechanism of a membrane-trafficking network. *Annu. Rev. Biophys. Biomol. Struct.* **35,** 277–298
11. Hurley, J. H., and Yang, D. (2008) MIT domainia. *Dev. Cell* **14,** 6–8
12. Babst, M., Katzmann, D. J., Estepa-Sabal, E. J., Meerloo, T., and Emr, S. D. (2002) ESCRT-III: an endosome-associated heterooligomeric protein complex required for MVB sorting. *Dev. Cell* **3,** 271–282
13. Shim, S., Kimpler, L. A., and Hanson, P. I. (2007) Structure/function analysis of four core ESCRT-III proteins reveals common regulatory role for extreme C-terminal domain. *Traffic* **8,** 1068–1079
14. Muzioł, T., Pineda-Molina, E., Ravelli, R. B., Zamborlini, A., Usami, Y., Göttlinger, H., and Weissenhorn, W. (2006) Structural basis for budding by the ESCRT-III factor CHMP3. *Dev. Cell* **10,** 821–830
15. Zamborlini, A., Usami, Y., Radoshitzky, S. R., Popova, E., Palu, G., and Göttlinger, H. (2006) Release of autoinhibition converts ESCRT-III components into potent inhibitors of HIV-1 budding. *Proc. Natl. Acad. Sci. U.S.A.* **103,** 19140–19145
16. Bajorek, M., Schubert, H. L., McCullough, J., Langelier, C., Eckert, D. M., Stubblefield, W. M., Uter, N. T., Myszka, D. G., Hill, C. P., and Sundquist, W. I. (2009) Structural basis for ESCRT-III protein autoinhibition. *Nat. Struct. Mol. Biol.* **16,** 754–762
17. Teis, D., Saksena, S., and Emr, S. D. (2008) Ordered assembly of the ESCRT-III complex on endosomes is required to sequester cargo during MVB formation. *Dev. Cell* **15,** 578–589
18. Saksena, S., Wahlman, J., Teis, D., Johnson, A. E., and Emr, S. D. (2009) Functional reconstitution of ESCRT-III assembly and disassembly. *Cell* **136,** 97–109
19. Hanson, P. I., Roth, R., Lin, Y., and Heuser, J. E. (2008) Plasma membrane deformation by circular arrays of ESCRT-III protein filaments. *J. Cell Biol.* **180,** 389–402
20. Wollert, T., Wunder, C., Lippincott-Schwartz, J., and Hurley, J. H. (2009) Membrane scission by the ESCRT-III complex. *Nature* **458,** 172–177
21. Nickerson, D. P., West, M., and Odorizzi, G. (2006) Did2 coordinates Vps4-mediated dissociation of ESCRT-III from endosomes. *J. Cell Biol.* **175,** 715–720
22. Azmi, I. F., Davies, B. A., Xiao, J., Babst, M., Xu, Z., and Katzmann, D. J. (2008) ESCRT-III family members stimulate Vps4 ATPase activity directly or via Vta1. *Dev. Cell* **14,** 50–61
23. Xiao, J., Xia, H., Zhou, J., Azmi, I. F., Davies, B. A., Katzmann, D. J., and Xu, Z. (2008) Structural basis of Vta1 function in the multivesicular body sorting pathway. *Dev. Cell* **14,** 37–49
24. Bajorek, M., Morita, E., Skalicky, J. J., Morham, S. G., Babst, M., and Sundquist, W. I. (2009) Biochemical analyses of human IST1 and its function in cytokinesis. *Mol. Biol. Cell* **20,** 1360–1373
25. Xiao, J., Chen, X. W., Davies, B. A., Saltiel, A. R., Katzmann, D. J., and Xu, Z. (2009) Structural basis of Ist1 function and Ist1-Did2 interaction in the multivesicular body pathway and cytokinesis. *Mol. Biol. Cell* **20,** 3514–3524
26. Nickerson, D. P., West, M., Henry, R., and Odorizzi, G. (2010) Regulators of Vps4 ATPase activity at endosomes differentially influence the size and rate of formation of intralumenal vesicles. *Mol. Biol. Cell* **21,** 1023–1032
27. Shestakova, A., Hanono, A., Drosner, S., Curtiss, M., Davies, B. A., Katzmann, D. J., and Babst, M. (2010) Assembly of the AAA ATPase Vps4 on ESCRT-III. *Mol. Biol. Cell* **21,** 1059–1071
28. Norgan, A. P., Davies, B. A., Azmi, I. F., Schroeder, A. S., Payne, J. A., Lynch, G. M., Xu, Z., and Katzmann, D. J. (2013) Relief of autoinhibition enhances Vta1 activation of Vps4 via the Vps4 stimulatory element. *J. Biol. Chem.* **288,** 26147–26156
29. Babst, M., Wendland, B., Estepa, E. J., and Emr, S. D. (1998) The Vps4p AAA ATPase regulates membrane association of a Vps protein complex required for normal endosome function. *EMBO J.* **17,** 2982–2993
30. Fujita, H., Yamanaka, M., Imamura, K., Tanaka, Y., Nara, A., Yoshimori, T., Yokota, S., and Himeno, M. (2003) A dominant negative form of the AAA ATPase SKD1/VPS4 impairs membrane trafficking out of endosomal/lysosomal compartments: class E vps phenotype in mammalian cells. *J. Cell Sci.* **116,** 401–414
31. Azmi, I., Davies, B., Dimaano, C., Payne, J., Eckert, D., Babst, M., and Katzmann, D. J. (2006) Recycling of ESCRTs by the AAA-ATPase Vps4 is regulated by a conserved VSL region in Vta 1. *J. Cell Biol.* **172,** 705–717
32. Ward, D. M. (2005) The role of LIP5 and CHMP5 in multivesicular body formation and HIV-1 budding in mammalian cells. *J. Biol. Chem.* **280,** 10548–10555
33. Scott, A. (2005) Structural and mechanistic studies of VPS4 proteins. *EMBO J.* **24,** 3658–3669
34. Scott, A., Gaspar, J., Stuchell-Brereton, M. D., Alam, S. L., Skalicky, J. J., and Sundquist, W. I. (2005) Structure and ESCRT-III protein interactions of the MIT domain of human VPS4A. *Proc. Natl. Acad. Sci. U.S.A.* **102,** 13813–13818
35. Skalicky, J. J., Arii, J., Wenzel, D. M., Stubblefield, W. M., Katsuyama, A., Uter, N. T., Bajorek, M., Myszka, D. G., and Sundquist, W. I. (2012) Interactions of the human LIP5 regulatory protein with endosomal sorting complexes required for transport. *J. Biol. Chem.* **287,** 43910–43926
36. Rue, S. M., Mattei, S., Saksena, S., and Emr, S. D. (2008) Novel Ist1-Did2 complex functions at a late step in multivesicular body sorting. *Mol. Biol. Cell* **19,** 475–484
37. Dimaano, C., Jones, C. B., Hanono, A., Curtiss, M., and Babst, M. (2008) Ist1 regulates Vps4 localization and assembly. *Mol. Biol. Cell* **19,** 465–474
38. Agromayor, M., Carlton, J. G., Phelan, J. P., Matthews, D. R., Carlin, L. M., Ameer-Beg, S., Bowers, K., and Martin-Serrano, J. (2009) Essential role of hIST1 in cytokinesis. *Mol. Biol. Cell* **20,** 1374–1387
39. Renvoisé, B., Parker, R. L., Yang, D., Bakowska, J. C., Hurley, J. H., and Blackstone, C. (2010) SPG20 protein spartin is recruited to midbodies by ESCRT-III protein Ist1 and participates in cytokinesis. *Mol. Biol. Cell* **21,** 3293–3303

40. Ciccarelli, F. D., Proukakis, C., Patel, H., Cross, H., Azam, S., Patton, M. A., Bork, P., and Crosby, A. H. (2003) The identification of a conserved domain in both spartin and spastin, mutated in hereditary spastic paraplegia. *Genomics* **81,** 437–441
41. Salinas, S., Proukakis, C., Crosby, A., and Warner, T. T. (2008) Hereditary spastic paraplegia: clinical features and pathogenetic mechanisms. *Lancet Neurol.* **7,** 1127–1138
42. Patel, H., Cross, H., Proukakis, C., Hershberger, R., Bork, P., Ciccarelli, F. D., Patton, M. A., McKusick, V. A., and Crosby, A. H. (2002) SPG20 is mutated in Troyer syndrome, an hereditary spastic paraplegia. *Nat. Genet.* **31,** 347–348
43. Renvoisé, B., Stadler, J., Singh, R., Bakowska, J. C., and Blackstone, C. (2012) $Spg20^{-/-}$ mice reveal multimodal functions for Troyer syndrome protein spartin in lipid droplet maintenance, cytokinesis and BMP signaling. *Hum. Mol. Genet.* **21,** 3604–3618
44. Eastman, S. W., Yassaee, M., and Bieniasz, P. D. (2009) A role for ubiquitin ligases and Spartin/SPG20 in lipid droplet turnover. *J. Cell Biol.* **184,** 881–894
45. Stuchell-Brereton, M. D., Skalicky, J. J., Kieffer, C., Karren, M. A., Ghaffarian, S., and Sundquist, W. I. (2007) ESCRT-III recognition by VPS4 ATPases. *Nature* **449,** 740–744
46. Obita, T., Saksena, S., Ghazi-Tabatabai, S., Gill, D. J., Perisic, O., Emr, S. D., and Williams, R. L. (2007) Structural basis for selective recognition of ESCRT-III by the AAA ATPase Vps4. *Nature* **449,** 735–739
47. Kieffer, C., Skalicky, J. J., Morita, E., De Domenico, I., Ward, D. M., Kaplan, J., and Sundquist, W. I. (2008) Two distinct modes of ESCRT-III recognition are required for VPS4 functions in lysosomal protein targeting and HIV-1 budding. *Dev. Cell* **15,** 62–73
48. Yang, D., Rismanchi, N., Renvoisé, B., Lippincott-Schwartz, J., Blackstone, C., and Hurley, J. H. (2008) Structural basis for midbody targeting of spastin by the ESCRT-III protein CHMP1B. *Nat. Struct. Mol. Biol.* **15,** 1278–1286
49. Samson, R. Y., Obita, T., Freund, S. M., Williams, R. L., and Bell, S. D. (2008) A role for the ESCRT system in cell division in archaea. *Science* **322,** 1710–1713
50. Solomons, J., Sabin, C., Poudevigne, E., Usami, Y., Hulsik, D. L., Macheboeuf, P., Hartlieb, B., Göttlinger, H., and Weissenhorn, W. (2011) Structural basis for ESCRT-III CHMP3 recruitment of AMSH. *Structure* **19,** 1149–1159
51. Yang, Z., Vild, C., Ju, J., Zhang, X., Liu, J., Shen, J., Zhao, B., Lan, W., Gong, F., Liu, M., Cao, C., and Xu, Z. (2012) Structural basis of molecular recognition between ESCRT-III-like protein Vps60 and AAA-ATPase regulator Vta1 in the multivesicular body pathway. *J. Biol. Chem.* **287,** 43899–43908
52. Vild, C. J., and Xu, Z. (2014) Vfa1 binds to the N-terminal microtubule-interacting and trafficking (MIT) domain of Vps4 and stimulates its ATPase activity. *J. Biol. Chem.* **289,** 10378–10386
53. Adams, P. D., Afonine, P. V., Bunkóczi, G., Chen, V. B., Davis, I. W., Echols, N., Headd, J. J., Hung, L. W., Kapral, G. J., Grosse-Kunstleve, R. W., McCoy, A. J., Moriarty, N. W., Oeffner, R., Read, R. J., Richardson, D. C., Richardson, J. S., Terwilliger, T. C., and Zwart, P. H. (2010) PHENIX: a comprehensive Python-based system for macromolecular structure solution. *Acta Crystallogr. D Biol. Crystallogr.* **66,** 213–221
54. Emsley, P., and Cowtan, K. (2004) Coot: model-building tools for molecular graphics. *Acta Crystallogr. D Biol. Crystallogr.* **60,** 2126–2132